



Short communication

Tunable electrical conductivity of a new 3D MOFs: Cu-TATAB

Qing-Qing Huang^{a,b}, Yang-Jie Lin^a, Rui Zheng^{a,b}, Wei-Hua Deng^a, Chiranjeevulu Kashi^a, P. Naresh Kumar^a, Guan-E Wang^{a,b,*}, Gang Xu^{a,b,*}

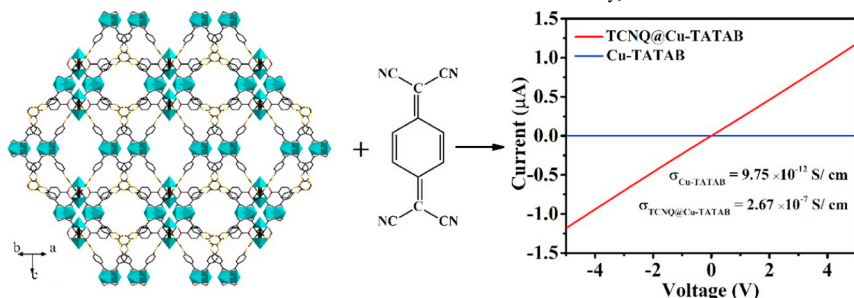
^a State Key Laboratory of Structural Chemistry, Fujian Institute of Research on the Structure of Matter, Chinese Academy of Sciences, Fuzhou 350002, China

^b University of Chinese Academy of Sciences, Chinese Academy of Sciences, Beijing 100039, China



GRAPHICAL ABSTRACT

A new three dimensional metal-organic frameworks composed of Cu^{2+} centres and polyacid linkers (TATAB^{3-}) was synthesized by solvothermal method, which contains two types of Cu_{24} cages. The conductivity of the Cu-MOF was increased by 4 orders of magnitude after doping with TCNQ molecules. This method realized the transformation of Cu-MOF from insulator to semiconductor. Finally, the Conductive mechanism of the doped Cu-MOF has been studied.



ARTICLE INFO

Keywords:

Metal-organic frameworks
Insulator
Semiconductor
TCNQ

ABSTRACT

Metal-organic frameworks (MOFs) are a kind of functional porous materials with the potential applications in gas adsorption and separation, catalysis, energy storage, sensor, and electrical conductivity. However, the insulating nature of the mostly MOFs limits their application in the electronic field. A new three-dimensional (3D) metal-organic framework composed of Cu^{2+} centres and polyacid linkers (TATAB^{3-}) was synthesized by solvothermal method, which contains two types of Cu_{24} cages. The crystal structure is cubic and each Cu is coordinated by five oxygen atoms which can be confirmed by the single crystal X-ray diffraction, infrared spectra and TGA analysis. The conductivity for this 3D MOF is increased by four orders of magnitude after doping with 7,7,8,8-tetracyanoquinodimethane (TCNQ) and realizes the transformation from an insulator to semiconductor.

1. Introduction

Metal-organic frameworks (MOFs) are a kind of multifunctional porous material with the advantages of high porosity, low density, large specific surface area, regular porous channel, adjustable pore size, and diverse topological structures [1–5], have attracted the attention of scientists owing to their potential applications in gas adsorption and

separation [6–8], catalysis [9], energy storage [10], sensor [11–13] and electrical conductivity [14,15]. The tunability and modifiability of both metal sites and organic ligands the extraordinary diversity and multifunction in framework structure and porosity [16–18]. Among the numerous excellent properties of MOFs, the seeking of conductive MOFs has become the hot topic. In the past decade, a few MOFs with high conductivity such as Cu-CAT, Ni-HITP, Cu-HITP and Cu-TCNQ have

* Corresponding authors at: State Key Laboratory of Structural Chemistry, Fujian Institute of Research on the Structure of Matter, Chinese Academy of Sciences, Fuzhou 350002, China.

E-mail addresses: gewang@fjirsm.ac.cn (G.-E. Wang), gxu@fjirsm.ac.cn (G. Xu).

<https://doi.org/10.1016/j.inoche.2019.04.037>

Received 12 April 2019; Received in revised form 24 April 2019; Accepted 26 April 2019

Available online 26 April 2019

1387-7003/ © 2019 Elsevier B.V. All rights reserved.

been explored and used in the applications of gas sensors [19,20], supercapacitors [21], lithium-sulfur batteries [22] and field effect transistors [23,24]. However, most of MOFs are known to be poor conductor due to the lack of transport channel of charge carrier between metal sites and organic ligands [25–27]. Hence, how to improve the conductivity of MOFs is became an important issue.

Many strategies such as composite structure, post-synthetic modification, filling of guest molecules and hybridized with other conductive media have been explored to improve the conductivity of MOFs [28–33]. Doping with redox active molecules is one of the efficient ways to enhance the conductivity of MOFs [34–37]. TCNQ (7,7,8,8-tetracyanoquinodimethane), a good electron acceptor molecule, can enhance the conductivity of MOFs through the formation of charge transfer complex within framework due to its high electron affinity [38]. Talin et al. have successfully improved the conductivity of $\text{Cu}_3(\text{BTC})_2$ by 6 orders of magnitude through introducing TCNQ into the framework [39]. Later, Sengupta and co-workers reported the same method to enhance the conductivity of metal-organic framework [Cu(TPyP)Cu₂(O₂CCH₃)₄] [40]. Thanks to the formation of charge transfer complex between the Cu-MOF and TCNQ, the conductivity of the as-fabricated TCNQ doped Cu-MOF thin film is increased. Thus, a multifunctional MOF with good conductivity might be designed and created.

Herein, we report the synthesis, crystal structure and characterization of a 3D MOF, [Cu₂(TATAB)₃]·7.5H₂O (Cu-TATAB), as well as its electrical conductivity influenced by TCNQ molecules. Cu-TATAB was synthesized by Cu²⁺ and TATAB³⁻, which shows insulation at room temperature (RT) with the conductivity of $9.75 \times 10^{-12} \text{ S cm}^{-1}$. It is noteworthy that the conductivity of Cu-TATAB was increased by > 4 orders of magnitude after doping with TCNQ.

2. Experimental

2.1. Materials

All solvents and reagents were purchased commercially and used without further purification. 4,4',4''-(1,3,5-Triazine-2,4,6-triyl)tris (azane diyl) tribenzoic acid (H₃TATAB) was purchased from J&K China Chemical Ltd. (China). Copper nitrate trihydrate (Cu(NO₃)₂·3H₂O) was purchased from Aladdin (USA). Acetic acid glacial was purchased from Tianjin Fuyu Fine Chemical Co., Ltd. (China). N,N-Dimethylformamide (DMF) and methanol (MeOH) were purchased from Sinopharm Group Co., Ltd. (China). TCNQ was purchased from Tokyo Chemical Industry Co., Ltd. (Japan). Water was purified using the Milli-Q purification system.

2.2. Synthesis of Cu-TATAB crystals

Cu(NO₃)₂·3H₂O (0.2 mmol, 25.4 mg), H₃TATAB (0.1 mmol, 25.7 mg), DMF (5 mL), H₂O (3 mL) and MeOH (2 mL) were placed in a 25 mL Teflon-lined reaction vessel, and then 350 μL acetic acid was added into the mix solution. The reaction vessel was placed in an oven and heated at 125 °C for 72 h, and then cooled to RT over 24 h. The green crystals were collected and washed by DMF for 4 times. In order to activate Cu-TATAB crystal, the resulting green crystals were soaked in methanol for one week to remove the solvent inside in the channel. Elemental analysis calcd.: C, 42.88%; H, 3.60%; N, 12.54%; O, 26.85%. Found: C, 42.96%; H, 3.49%; N, 12.52%; O, 26.82%.

2.3. X-ray crystal structure determinations

Single crystal X-ray diffraction data of compound Cu-TATAB were collected on a SuperNova diffractometer (Rigaku, Japan) with the Mo K α radiation ($\lambda = 0.71073 \text{ \AA}$). The crystal was kept at 100.01(10) K during data collection. The structure of Cu-TATAB was determined by direct method and refined on F^2 by full-matrix least-squares method using the SHELXTL-2015 program package [37]. The X-ray diffraction

Table 1
Crystal data and structure refinement for Cu-TATAB.

| Crystal data | Cu-TATAB |
|---|---|
| Empirical formula | C ₃₂ H ₂₁ Cu ₂ N ₈ O ₁₀ |
| Formula weight | 804.65 |
| Temperature | 100 (10) K |
| Wavelength | 0.71073 |
| Crystal system | Cubic |
| Space group | <i>Im</i> -3 |
| Unit cell dimensions | $a = 27.9468(7) \text{ \AA}$, $\alpha = 90^\circ$ $b = 27.9468(7) \text{ \AA}$, $\beta = 90^\circ$ $c = 27.9468(7) \text{ \AA}$, $\gamma = 90^\circ$ |
| Volume | 21,827.1(16) \AA^3 |
| Z | 12 |
| F(000) | 4884.0 |
| Limiting indices | $-22 \leq h \leq 36$ $-37 \leq k \leq 14$ $-33 \leq l \leq 38$ |
| Reflections collected | 15,773 |
| Independent reflections | 4514 |
| Completeness | 99.83% |
| D_c | 0.704 g/cm ³ |
| μ | 0.617 mm ⁻¹ |
| R_{int} | 0.0539 |
| R_1 values [$I \geq 2\sigma(I)$] | 0.0887 |
| w R_2 [all data] | 0.2985 |
| GOF on F^2 | 1.031 |
| $R_1 = \sum F_o - F_c / \sum F_o $, w $R_2 = \sum (F_o ^2 - F_c ^2) / \sum F_o ^2$ | |

crystallographic data and structure refinements for Cu-TATAB are demonstrated in Table 1, and the bond distances and angles are given in Tables S1 and S2. Crystallographic data for Cu-TATAB reported in this paper have been deposited in the Cambridge Crystallographic Data Centre with CCDC 1908714. This data can be obtained free of charge from the Cambridge Crystallographic Data Centre via www.ccdc.cam.ac.uk/data_request/cif.

2.4. Characterization

The powder X-ray diffraction (PXRD) patterns were recorded on a Rigaku MiniFlex600 diffractometer using Cu K α radiation. The Fourier transform infrared spectroscopy (FT-IR) spectra were recorded on a Bruker VERTEX70 FT-IR spectrometer (Germany) in 4000–400 cm⁻¹ region using KBr pellets. Thermogravimetric analyses were done on a NETZSCHSTA449C analyzer (Germany) with a heating rate of 10 °C min⁻¹ from 25 to 800 °C, with a N₂ flow rate of 20 mL min⁻¹. UV-vis-NIR absorbance spectra were recorded on a Lambda 950 (PerkinElmer, USA) using BaSO₄ as a standard. The electrical measurements were performed using a Keithley 4200 (USA).

3. Results and discussion

Crystals of Cu-TATAB were prepared in a solvothermal reaction of Cu(NO₃)₂·3H₂O and H₃TATAB in H₂O/DMF/MeOH (v/v/v = 3:5:2) at 125 °C. The product was isolated as green crystals.

Single-crystal X-ray diffraction studies reveal that Cu-TATAB crystallizes in cubic space group *Im*-3. As shown in Fig. 1a, there are two Crystallographic independent Cu^{II} atoms, which has the same coordination number of 5. Each Cu atom exhibits tetragonal pyramid geometry coordinated by five oxygen atoms to form the well-known paddlewheel secondary building unit (SBU) with a short Cu–Cu distance of 2.606(13) \AA [41]. The Cu–O distances range from 1.938(3) to 1.944(4) \AA , that are similar to those of reported in the literatures [42]. The existent of three amino groups in the TATAB³⁻ ligand, resulting to the repulsion between hydrogen atoms derive from those amino group and peripheral rings, allowing for the distortion of TATAB³⁻ in Cu-TATAB as shown in Fig. 1b [43]. The dihedral angle between the peripheral ring and the central ring is 33.4° (Fig. S1). Different from the

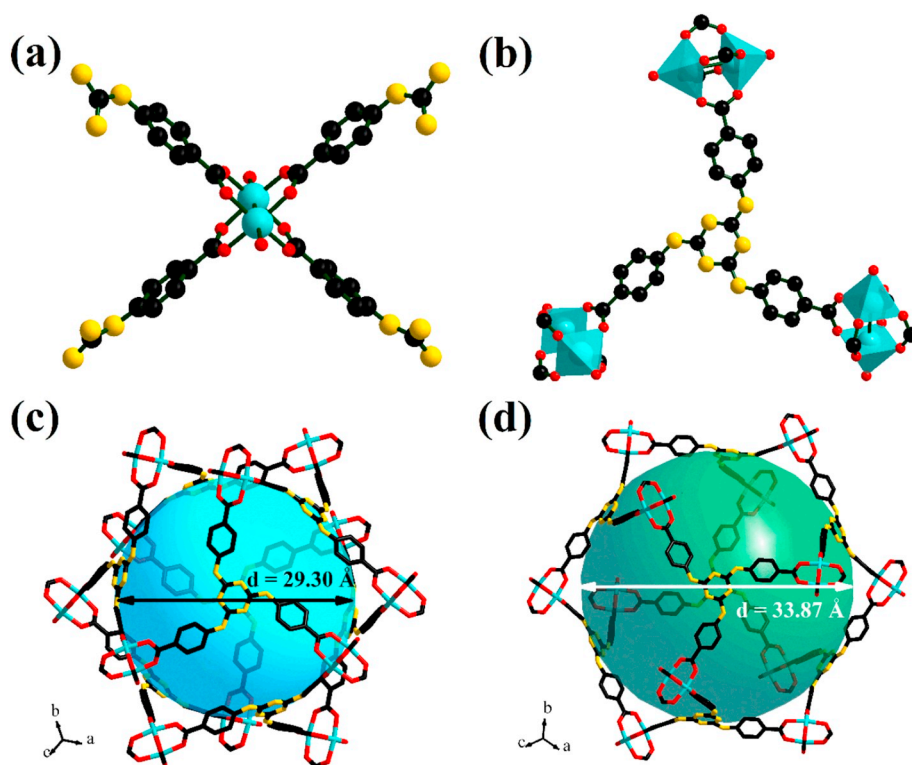


Fig. 1. (a) A paddlewheel structure unit of Cu-TATAB (cyan, red, black and yellow spheres represent the Cu, O, C and N atoms, respectively.). (b) Coordination mode of TATAB ligand in Cu-TATAB. (c) An icosahedral Cu₂₄-A cage. The blue sphere represents the void inside the cage. (d) An icosahedral Cu₂₄-B cage. The green sphere represents the void inside the cage. (For interpretation of the references to color in this figure legend, the reader is referred to the web version of this article.)

reported mesoMOF-1 [44], each SBU structure connects four TATAB³⁻ ligands, and each TATAB³⁻ ligand binds three SBUs to form an icosahedral Cu₂₄ cage (Fig. 1c and d), where all twelve vertices are taken up by the SBUs, and eight of the twenty faces are occupied by TATAB³⁻ ligands. It is noteworthy that there are two types of Cu₂₄ cages in Cu-TATAB, the diameters of cages Cu₂₄-A and Cu₂₄-B are 29.30 Å and 33.87 Å, respectively.

The 3D packing structure of Cu-TATAB along the [100] and [110] directions are shown in Fig. 2, the CuO₅ tetragonal pyramid is linker with TATAB⁻ ligand to form the porous structure. Open microchannels of Cu-TATAB from all three orthogonal directions with the same shape of a hexagon and the same size as large as 27.9 × 16.5 Å (Fig. 2a). There are two kinds of channels along the [110] direction in Cu-TATAB, in which the rhombic and hexagon channels are with the approximate sizes of 11.98 × 8.47 Å and 9.76 × 8.47 Å, respectively, without taking the van der Waals radius into consideration.

The phase purity of Cu-TATAB bulk sample was confirmed by PXRD. As shown in Fig. 3a, all of the peaks of experiment pattern are well consistent with the simulated PXRD pattern, which indicated the high

purity of Cu-TATAB sample. In order to investigate the coordination of Cu(II) and TATAB³⁻ ligand in compound Cu-TATAB, we measured the FT-IR spectroscopy as shown in Fig. 3b. Compared with the H₃TATAB ligand, the disappearance of the strong absorption from 3500 to 2400 cm⁻¹ (O–H stretching vibration) in IR spectroscopy indicated the coordination of Cu(II) ions and TATAB ligands [45]. Both the H₃TATAB and compound Cu-TATAB showed prominent peaks in the 1590–1700 cm⁻¹ region that can be assigned as a contribution of C=C and C=O stretching modes [46]. The peak at 3400 cm⁻¹ of the Cu-TATAB, arising from the –NH-stretching vibration, which indicates that the amino group in TATAB³⁻ ligand is not participating in coordination [47]. Furthermore, the thermal gravimetric analysis (TGA) of as-synthesized Cu-TATAB was investigated under a nitrogen atmosphere (Fig. 3c). The curve of Cu-TATAB shows a rapid weight loss of about 10% before the temperature of 100 °C, corresponding to the loss of H₂O molecules inside the channels (calc. 10.07%). The abrupt decrease at 300 °C in the TGA curve suggests decomposition of the complex above this temperature. The solid-state UV–vis-NIR absorbance spectra of the Cu-TATAB and the ligand show abroad absorbance extending across the

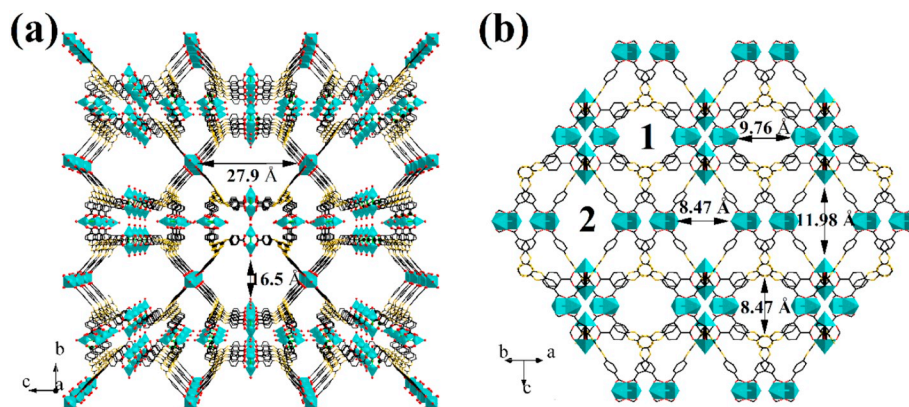


Fig. 2. (a) A view of packing of Cu-TATAB from the [100] direction. (b) Two types of channels in Cu-TATAB.

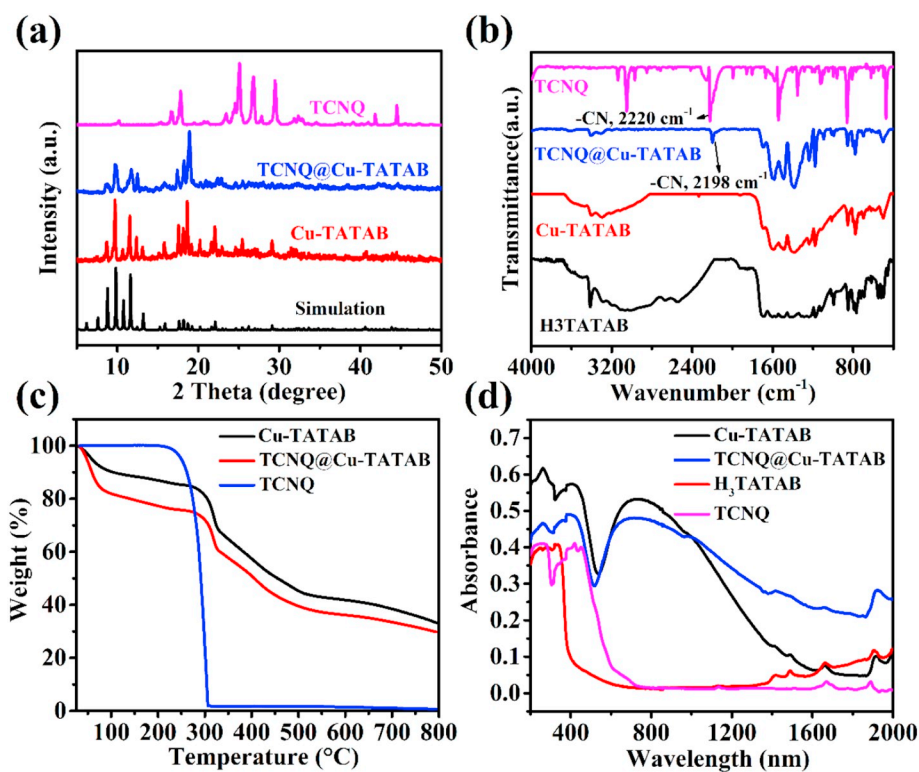


Fig. 3. (a) PXRD patterns of Cu-TATAB, TCNQ@Cu-TATAB and TCNQ. (b) FT-IR spectra of Cu-TATAB, H₃TATAB, TCNQ@Cu-TATAB and TCNQ. (c) TG curves of Cu-TATAB, TCNQ@Cu-TATAB and TCNQ. (d) UV-vis-NIR absorption of Cu-TATAB, H₃TATAB, TCNQ@Cu-TATAB and TCNQ.

range of 200–1800 nm⁻¹ and 200–800 nm, respectively. As shown in Fig. 3d, Cu-TATAB shows two additional broad absorption bands in the visible region at 417 nm and 729 nm. The higher energy band (at 417 nm) can be ascribed to the metal-to-ligand charge transfer (MLCT)

transitions, while the lower energy band (at 729 nm) may due to the d-d transitions of copper(II) compounds [48–51].

As shown in Fig. 4a, when the activated Cu-TATAB was soaked in the methanol solution of TCNQ for 3 days, the color of the crystal

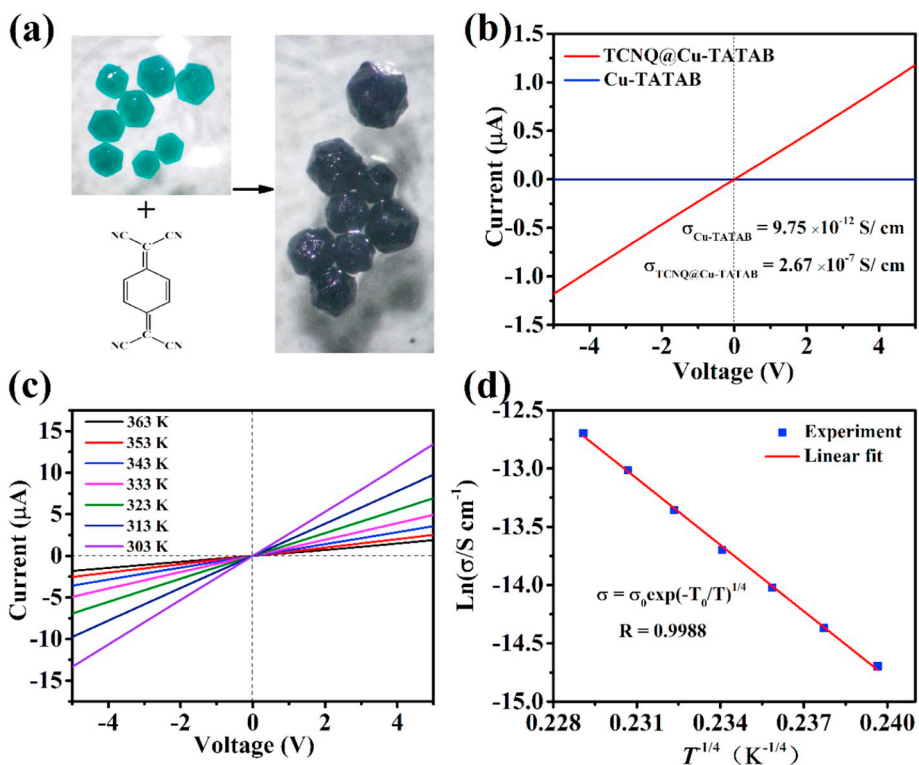


Fig. 4. (a) Color change of Cu-TATAB before and after doping with TCNQ (b) IV curves of Cu-TATAB before and after TCNQ participated. (c) Temperature-dependent I-V curves of TCNQ@Cu-TATAB. (d) Mott variable-range hopping fit of $\ln\sigma$ vs $T^{-1/4}$ plot for $d = 3$.

changed from green to dark. PXRD analyses showed that before and after doping with TCNQ, they have similar crystal structures (Fig. 3a). The FT-IR pattern of Cu-TATAB before and after TCNQ doping was shown in Fig. 3b, the $-\text{CN}$ stretching frequency appeared at 2198 cm^{-1} indicated that TCNQ was successfully doped in Cu-TATAB, while the $-\text{N}$ stretching peak of TCNQ appears at 2220 cm^{-1} . The blue shift of the infrared peak of $-\text{CN}$ is due to the coordination between TCNQ and Cu-TATAB which cause the transformation of TCNQ molecules from neutral TCNQ to TCNQ ion [52]. TGA curves of Cu-TATAB and TCNQ@Cu-TATAB were shown in Fig. 3c, more weight loss of TCNQ@Cu-TATAB compared with Cu-TATAB indicated that TCNQ molecules were entered in the channel of Cu-TATAB. The UV-vis-NIR absorption spectra of TCNQ@Cu-TATAB showed a clear blue shift at the peak of 677 nm compared to Cu-TATAB. The new, broad absorption band at $900\text{--}1400\text{ nm}$ may be caused by the formation of charge transfer complex of TCNQ and Cu-TATAB.

A two probe method [53] was used to investigate the electrical properties of Cu-TATAB and TCNQ@Cu-TATAB by a pressed pellet where both faces of the pellet were painted with silver paint. As shown in Fig. 4b, RT measurement of Cu-TATAB at air condition exhibited very low conductivity of $9.75 \times 10^{-12}\text{ S cm}^{-1}$, which is consistent with its insulating nature. After doping with TCNQ molecules, the conductivity of TCNQ@Cu-TATAB increases to $2.67 \times 10^{-7}\text{ S cm}^{-1}$ at RT, which is more than four orders of magnitude higher than that of Cu-TATAB. As shown in Fig. 4c, the good linear relationship between current and voltage indicated good ohmic contacts between TCNQ@Cu-TATAB and electrodes. The conductivity of TCNQ@Cu-TATAB shows a monotonic increase with the rise of temperature and reaches to $3.06 \times 10^{-6}\text{ S cm}^{-1}$ at 363 K . The increase of Cu-TATAB conductivity is contributed to the participation of TCNQ molecules formed localized conducting regions in Cu-TATAB, which can be explained by mott's variable-range hopping (M-VRH) mode [54,55]. According to this theory, the charge transport between localized states near the Fermi level E_F is controlled by the jump of localized electrons. The conductivity of d-dimensional sample follows the expression of temperature (T) $\sigma(T) = \sigma_0 \exp(-T_0/T)^{1/d+1}$. As shown in Fig. 4d, the logarithmic conductivity σ agrees well with the $d = 3$ M-VRH mode and shows good linear with $T^{1/4}$, which indicated the transformation from insulator to semiconductor of Cu-TATAB. The insertion of the unoccupied molecular orbitals of TCNQ molecules in the HOMO-LUMO gap of compound formed a charge transport channel within the Cu-TATAB, which makes it possible for the electrons to jump from one localized state to another localized state under the applied external electrical field [40].

4. Conclusion

In conclusion, the 3-D porous structure of Cu-TATAB has been revealed by using powder X-ray diffraction data. The FT-IR spectrum of the title compound has confirmed the coordination of the deprotonation of the carboxyl group and the Cu(II) ion, while the amino groups in this framework are not participated in coordination. The conductivity of Cu-TATAB was increased by > 4 orders of magnitude after doping with TCNQ. The transformation of Cu-TATAB from an insulator to semiconductor indicated that TCNQ doping is an effective method to improve the conductivity of none-conductive MOFs.

Acknowledgements

This work was supported by National Natural Science Foundation of China (201805276), the Funds for International Cooperation and Exchange of the National Natural Science Foundation of China (21850410462), the National Science Foundation for Post-doctoral Scientists of China (2018M642576, 2018M642578), Natural Science Foundation of Fujian Province (2017J05034), Youth Innovation Promotion Association CAS.

References

- [1] Y.L. Hou, M.Q. Li, S.X. Cheng, Y.X. Diao, F. Vilela, Y.H. He, J. He, Z.T. Xu, Chem. Commun. 54 (2018) 9470–9473.
- [2] Z.Y. Li, Z.J. Zhang, Y.X. Ye, K.C. Cai, F.F. Du, H. Zeng, J. Tao, Q.J. Lin, Y. Zheng, S.C. Xiang, J. Mater. Chem. A 5 (2017) 7816–7824.
- [3] J.S. Qin, S. Yuan, L. Zhang, B. Li, D.Y. Du, N. Huang, W. Guan, H.F. Drake, J.D. Pang, Y.Q. Lan, A. Alsalmeh, H.C. Zhou, J. Am. Chem. Soc. 141 (2019) 2054–2060.
- [4] Y.Z. Chen, R. Zhang, L. Jiao, H.L. Jiang, Coord. Chem. Rev. 362 (2018) 1–23.
- [5] X.N. Mi, D.F. Sheng, Y.E. Yu, Y.H. Wang, L.M. Zhao, J. Lu, Y.W. Li, D.C. Li, J.M. Dou, J.G. Duan, S.N. Wang, ACS Appl. Mater. Interfaces 11 (2019) 7914–7926.
- [6] J.D. Evans, B. Garai, H. Reinsch, W.J. Li, S. Dissegna, V. Bon, I. Senkowska, R.A. Fischer, S. Kaskel, C. Janiak, N. Stock, D. Volkmer, Coord. Chem. Rev. 380 (2019) 378–418.
- [7] D.X. Xue, Q. Wang, J.F. Bai, Coord. Chem. Rev. 378 (2019) 2–16.
- [8] S.S. Zhang, X. Wang, H.F. Su, L. Feng, Z. Wang, W.Q. Ding, V.A. Blatov, M. Kurmoo, C.H. Tung, D. Sun, L.S. Zheng, Inorg. Chem. 56 (2017) 11891–11899.
- [9] S. Yuan, L. Feng, K.C. Wang, J.D. Pang, M. Bosch, C. Lollar, Y.J. Sun, J.S. Qin, X.Y. Yang, P. Zhang, Q. Wang, L.F. Zou, Y.M. Zhang, L.L. Zhang, Y. Fang, J.L. Li, H.C. Zhou, Adv. Mater. 37 (2018) 1704303.
- [10] A. Indra, T. Song, U. Paik, Adv. Mater. 39 (2018) 1705146.
- [11] D. Liu, J.W. Wan, G.S. Pang, Z.Y. Tang, Adv. Mater. (2018) 1803291.
- [12] W.M. Chen, X.L. Meng, G.L. Zhuang, Z. Wang, M. Kurmoo, Q.Q. Zhao, X.P. Wang, B.R. Shan, C.H. Tung, D. Sun, J. Mater. Chem. A 5 (2017) 13079–13085.
- [13] Z.W. Chen, X.N. Mi, J. Lu, S.N. Wang, Y.W. Li, J.M. Dou, D.C. Li, Dalton Trans. 47 (2018) 6240–6249.
- [14] W.W. Zhao, J.L. Peng, W.K. Wang, S.J. Liu, Q. Zhao, W. Huang, Coord. Chem. Rev. 377 (2018) 44–63.
- [15] X.Y. Li, H.F. Su, M. Kurmoo, C.H. Tung, D. Sun, L.S. Zheng, Nanoscale 9 (2017) 5305–5314.
- [16] A. Kirchner, L. Feng, H.F. Drake, E.A. Joseph, H.C. Zhou, Chem. Soc. Rev. 23 (2018) 8611–8638.
- [17] N.A. Khan, Z. Hasan, S.H. Jung, Coord. Chem. Rev. 376 (2018) 20–45.
- [18] Z. Hassan, E. Spuling, D.M. Knoll, J. Lahann, S. Bräse, Chem. Soc. Rev. 47 (2018) 6947–6963.
- [19] V.R. Giménez, N.A. Barrios, G.E. Ariza, M. Galbiati, M. Sessolo, S. Tatay, C.M. Gastaldo, Angew. Chem. Int. Ed. 57 (2018) 15086–15090.
- [20] M.G. Campbell, D. Sheberla, S.F. Liu, T.M. Swager, M. Dincă, Angew. Chem. 127 (2015) 4423–4426.
- [21] W.H. Li, K. Ding, H.R. Tian, M.S. Yao, B. Nath, W.H. Deng, Y.B. Wang, G. Xu, Adv. Funct. Mater. 27 (2017) 1702067.
- [22] Y. Zang, F. Pei, J.H. Huang, Z.H. Fu, G. Xu, X.L. Fang, Adv. Energy Mater. 31 (2018) 1802052.
- [23] R. Basori, A.K. Raychaudhuri, J. Phys. Chem. C 122 (2018) 1054–1060.
- [24] G.D. Wu, J.H. Huang, Y. Zang, J. He, G. Xu, J. Am. Chem. Soc. 139 (2017) 1360–1363.
- [25] S.K. Bhardwaj, N. Bhardwaj, R. Kaur, J. Mehta, A.L. Sharma, K.H. Kim, A. Deep, J. Mater. Chem. A 6 (2018) 14992.
- [26] L. Sun, M.G. Campbell, M. Dincă, Angew. Chem. Int. Ed. 55 (2016) 3566–3579.
- [27] D.M. D'Alessandro, J.R. Kanga, J.S. Caddy, Aust. J. Chem. 64 (2011) 718–722.
- [28] N. Wang, T. Liu, H. Shen, S. Ji, J.R. Li, R. Zhang, AIChE J. 62 (2016) 538–546.
- [29] K.T. Butler, C.H. Hendon, A. Walsh, J. Am. Chem. Soc. 136 (2014) 2703–2706.
- [30] B. Li, M. Chrzanowski, Y. Zhang, S. Ma, Coord. Chem. Rev. 307 (2016) 106–129.
- [31] J. Lei, R. Qian, P. Ling, L. Cui, H. Ju, TrAC-Trend Anal. Chem. 58 (2014) 71–78.
- [32] M.G. Campbell, D. Sheberla, S.F. Liu, T.M. Swager, M. Dincă, Angew. Chem. Int. Ed. 54 (2015) 4349–4352.
- [33] M.L. Aubrey, B.M. Wiers, S.C. Andrews, T. Sakurai, S.E.R. Lillo, S.M. Hamed, C.J. Yu, L.E. Darago, J.A. Mason, J.O. Baeg, F. Grandjean, G.J. Long, S. Seki, J.B. Neaton, P.D. Yang, J.R. Long, Nat. Mater. 17 (2018) 625–632.
- [34] Z. Yin, Q.X. Wang, M.H. Zeng, J. Am. Chem. Soc. 134 (2012) 4857–4863.
- [35] M.H. Zeng, Q.X. Wang, Y.X. Tan, S. Hu, H.X. Zhao, L.S. Long, M. Kurmoo, J. Am. Chem. Soc. 132 (2010) 2561–2563.
- [36] Y. Kobayashi, B. Jacobs, M.D. Allendorf, J.R. Long, Chem. Mater. 22 (2010) 4120–4122.
- [37] G.M. Sheldrick, Acta Cryst. A 71 (2015) 3–8.
- [38] S.L. Cai, Y.B. Zhang, A.B. Pun, B. He, J. Yang, F.M. Toma, I.D. Sharp, O.M. Yaghi, J. Fan, S.R. Zheng, Chem. Sci. 5 (2014) 4693–4700.
- [39] A.A. Talin, A. Centrone, A.C. Ford, M.E. Foster, V. Stavila, P. Haney, R.A. Kinney, V. Szalai, F.E. Gabaly, H.P. Yoon, Science 343 (2014) 1246738.
- [40] A. Sengupta, S. Datta, C. Su, T.S. Herng, J. Ding, J.J. Vittal, K.P. Loh, ACS Appl. Mater. Interfaces 8 (2016) 16154–16159.
- [41] Y.H. Han, Z.Y. Zhou, C.B. Tian, S.W. Du, Green Chem. 18 (2016) 4086–4091.
- [42] Y. Song, R.Q. Fan, X. Du, K. Xing, P. Wang, Y.W. Dong, Y.L. Yang, CrystEngComm 18 (2016) 6411–6424.
- [43] R. Luebke, J.F. Eubank, A.J. Cairns, Y. Belmabkhout, L. Wojtas, M. Eddaoudi, Chem. Commun. 48 (2012) 1455–1457.
- [44] X.S. Wang, S.Q. Ma, D.F. Sun, S. Parkin, H.C. Zhou, J. Am. Chem. Soc. 128 (2006) 16474–16475.
- [45] N. Akai, S. Kudoh, M. Takayanagi, M. Nakata, J. Phys. Chem. A 106 (2002) 11029–11033.
- [46] L.F.C. de Oliveira, H.G.M. Dewards, E.S. Velozo, M. Nesbitt, Vib. Spectrosc. 28 (2002) 243–249.
- [47] L.C. Snoek, R.T. Kroemer, M.R. Hockridge, J.P. Simons, Phys. Chem. Phys. 3 (2001) 1819–1826.

- [48] L. Qin, Z.J. Wang, T. Wang, H.G. Zheng, J.X. Chen, Dalton Trans. 43 (2014) 12528–12535.
- [49] M.D. Hardi, C. Serre, T. Frot, L. Rozes, G. Maurin, C. Sanchez, G. Férey, J. Am. Chem. Soc. 131 (2009) 10857–10859.
- [50] J. Carranza, C. Brennan, J. Sletten, J.M. Clemente-Juan, F. Lloret, M. Julve, Inorg. Chem. 42 (2003) 8716–8727.
- [51] J.K. Nath, A. Mondal, A.K. Powell, J.B. Baruah, Cryst. Growth Des. 14 (2014) 4735–4748.
- [52] M. Inoue, M.B. Inoue, Inorg. Chem. 25 (1986) 37–41.
- [53] G.E. Wang, G. Xu, B.W. Liu, M.S. Wang, M.S. Yao, G.C. Guo, Angew. Chem. Int. Ed. 55 (2016) 514–518.
- [54] G. Givaja, P. Amo-Ochoa, C.J. Gómez-García, F. Zamora, Chem. Soc. Rev. 41 (2012) 115–147.
- [55] Y.F. Lin, W.B. Jian, C.P. Wang, Y.W. Suen, Z.Y. Wu, F.R. Chen, J.J. Kai, J.J. Lin, Appl. Phys. Lett. 90 (2007) 223117.